IEEE Access
Multidisciplinary | Rapid Review | Open Access Journal

Received August 27, 2020, accepted September 6, 2020, date of publication September 14, 2020,
date of current version September 25, 2020.

Digital Object Identifier 10.1109/ACCESS.2020.3024112

Operating Cost Reduction of DC Microgrids Under Real-Time Pricing Using Adaptive Differential Evolution Algorithm

XIAOYAN QIAN[1], (Student Member, IEEE), YUN YANG[2], (Member, IEEE), CHENDAN LI[3], (Member, IEEE), AND SIEW-CHONG TAN[1], (Senior Member, IEEE)

[1]Department of Electrical and Electronic Engineering, The University of Hong Kong, Hong Kong
[2]Department of Electrical Engineering, The Hong Kong Polytechnic University, Hong Kong
[3]Department of Electric Power Engineering, Norwegian University of Science and Technology, 7491 Trondheim, Norway

Corresponding author: Yun Yang (yun.1989yang@polyu.edu.hk)

ABSTRACT Virtual resistance-based droop control is widely adopted as secondary-layer control for grid-connected converters in DC microgrids. This paper presents an alternative usage of the virtual resistances to minimize the total operating cost of DC microgrids under real-time pricing. The total operating cost covers the running cost of utility grids, renewable energy sources (RES), energy storage systems (ESS), fuel cells, and power loss on the distribution lines. An adaptive Differential Evolution (ADE) algorithm is adopted in this paper to optimize the virtual resistances of the droop control for the grid-connected converters of dispatchable units, such that the power flow can be regulated. The performances of the proposed strategy are evaluated by the case studies of a 12-bus 380 V DC microgrid using Matlab and a 32-bus 380 V DC microgrid using a Real-Time Digital Simulator (RTDS). Both results validate that the ADE can significantly reduce the operating cost of DC microgrids and outperform the conventional Genetic Algorithm (GA) in terms of cost saving. Comparisons among the microgrids with different numbers of dispatchable units reveal that the cost saving is more prominent when the expansion of dispatchable units.

INDEX TERMS Adaptive differential evolution (ADE), DC microgrids, operating cost, virtual resistance.

I. INTRODUCTION

With high penetrations of renewable energy sources (RES), and energy storage systems (ESS), DC microgrids with on-site power generations are widely adopted in electric ships, data centers, smart buildings, island grids, and some residential communities, etc. [1]–[9]. Grid-connected converters are widely used for the integrations of utility grids, RES, ESS, fuel cells, and loads to the DC microgrids. To ensure stability, efficiency improvement, dynamic current sharing, state-of-charge (SoC) balance of battery storage systems, etc., droop control and its derivatives, owing to the merits of being communication-free and easy plug-and-play implementation, have been widely adopted for grid-connected converters [10]–[14]. In [10], a virtual resistance is introduced in the inner current control loop of the consensus control to achieve decentralized current sharing and enhance the system damping for the DC microgrid. In [11], an enhanced adaptive droop control scheme is proposed to further improve the current sharing accuracy and eliminate the DC voltage deviation by using both voltage-shifting and slope-adjusting approaches for the droop coefficients. In [12], an adaptive virtual resistance-based droop control is designed to balance the output current of distributed battery systems in DC microgrids. In [13], an adaptive droop control based on the n-th order of the SoC is proposed to balance the SoC of the energy storage units. In [14], a hierarchical control scheme based on variable bus voltages is proposed to mitigate distribution power loss in islanded DC microgrids. Virtual resistance is a critical concept of droop control to compensate the mismatch of external feeder impedance, and achieve accurate active power sharing in DC microgrids. However, investigations of controlling virtual resistances to effectively improve the economic profit

The associate editor coordinating the review of this manuscript and approving it for publication was Bin Zhou.

of DC microgrids are rarely conducted. In this paper, power flow between the utility grids, RES, ESS, fuel cells, loads and DC microgrids, respectively, and the power loss on the distribution lines are regulated by the control of virtual resistances. Considering the cost of the utility grids, RES, ESS, fuel cells, and the distribution power losses, electricity prices of DC microgrids can be minimized under real-time pricing and load profiles via the optimization of virtual resistances. The stability of DC microgrids is inherently guaranteed by the capacity limits of dispatchable units, tolerances of bus voltages, and constraints of virtual resistances in the objective function for the economic dispatch. This paper aims to minimize the total operating cost of DC microgrids by regulating the virtual resistances of the droop control for grid-connected converters and investigate the cost reduction performance when the dispatchable units are expanded.

By far, several pioneering research works have been carried out to reduce the operating cost of various DC microgrids [15]–[20]. In [15], cost-based dynamic droop gradients are included in the control scheme for distributed generators to produce more power from less costly generators. As a result, the overall generation cost in DC microgrids can be reduced without centralized control and communication links. In [16], a prioritized normalized cost algorithm is developed to reduce the generation cost for DC microgrids at light load conditions. In [17], a distributed sub-gradient algorithm is presented to reduce the generations of DC microgrids in both grid-connected and islanded modes. In [18], economic load sharing and power balance are simultaneously achieved by a distributed adaptive droop hierarchical control, which consists of secondary and tertiary controllers. In [19], a distributed cost optimization control scheme with the considerations of communication delay is addressed for islanded DC microgrids. In [20], the incremental cost of distributed generators is equalized by a fully distributed consensus-based optimizer. Nevertheless, the traditional methods of reducing operating cost in DC microgrids are struggling in finding global optimality with high computation complexity. This is because the numerical evaluation of the derivatives requires much computation, such as linear programming (LP) and nonlinear programming (NLP) by resorting to different relaxation methods of the underlying formulation [21]–[23]. Thereupon, prohibitive computation time is needed to find optimal solutions. Nevertheless, heuristic algorithms can find optimal solutions more efficient than conventional optimization techniques without sacrificing accuracy and running speed [24].

Several previous investigations on economic dispatches of DC microgrids using heuristic algorithms have been conducted [25]–[28]. In [25], a conventional Genetic Algorithm (GA) is adopted to reduce the operating cost of a six-bus DC microgrid incurred by the fuel and efficiency of the components and the demand response requirements from the utility grid. However, the operating cost of the DC microgrid may suffer from local optimization. In [26], a matrix real-coded GA is used to optimize the sizes, types, and locations of ESS based on the dynamic models and the net present values of DC microgrids. In [27], a distributed control algorithm is applied in isolated DC microgrids to enhance reliability and economic performance. However, the total operating cost of the DC microgrids is not considered. In [28], the countable operating cost of the resources in DC microgrids are qualified as fixed values while the uncountable counterparts are neglected. However, operating cost reduction of DC microgrids by heuristic algorithms has not been fully investigated. In this paper, an economic dispatch strategy under real-time pricing based on an adaptive Differential Evolution (ADE) algorithm is proposed to reduce the operating cost of DC microgrids with different numbers of buses. The economic dispatch concerns the operating cost of all the components, which includes the operating cost of the utility grid, RES, ESS, fuel cells, and distribution power lines, in DC microgrids. The total operating cost of the DC microgrids being optimized by the proposed ADE will be compared to that being optimized by the conventional GA method.

The main contributions of this paper include: (i) This might be the first paper to globally optimize the total operating cost of RES, ESS, fuel cells, loads, and distribution power loss in DC microgrids. The total operating cost of DC microgrids is minimized at different operating conditions. (ii) This paper reveals that the operating cost reduction is more prominent when more dispatchable units are connected to the DC microgrid, which has never been reported.

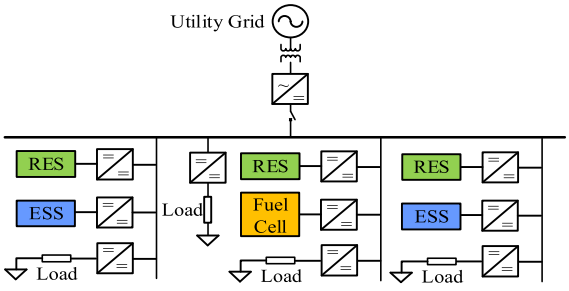

FIGURE 1. A typical architecture of DC microgrid.

II. OPERATING COST OF THE COMPONENTS

Fig. 1 shows a typical DC microgrid with the penetrations of the power supply by RES and the power demand by loads. The power supply and demand are balanced by the integrations of fuel cells, ESS, and the utility grid. Without considering any maintenance cost (which is neglible as compared to the operating cost), the operating cost of the components in the DC microgrid can be defined as follows:

A. UTILITY GRID COST

The operating cost of the utility grid is evaluated by the market price [4]. By utilizing smart meters, end-users can actively participate in the power regulation of DC microgrids as either power consumers or suppliers [29]. Therefore, the utility grid

cost can be expressed as

$$C_{\mathrm{U}} = \begin{cases} \dfrac{\lambda_{\mathrm{buy}} P_{\mathrm{U}}}{\Delta T}, & P_{\mathrm{U}} > 0 \\ \dfrac{\lambda_{\mathrm{sell}} P_{\mathrm{U}}}{\Delta T}, & P_{\mathrm{U}} < 0 \end{cases} \tag{1}$$

where λ_{buy} is the real-time buying electricity price of the utility grid; λ_{sell} is the real-time selling electricity price from the DC microgrid to the utility grid; P_{U} is the measured power flow between the DC microgrid and the utility grid; ΔT is the number of optimization cycles during one hour. In this paper, according to the suggestions given by the National Development and Reform Commission (NDRC) [30], the buying and selling electricity prices are the same (i.e., $\lambda_{\mathrm{buy}} = \lambda_{\mathrm{sell}}$).

B. ESS COST

The operating cost of ESS are modelled based on the charging and discharging efficiency [31],

$$C_{\mathrm{ESS}} = \begin{cases} \dfrac{\lambda_{\mathrm{buy}} \left(P_{\mathrm{ESS}} - \eta_{\mathrm{ch}} P_{\mathrm{ESS}}\right)}{\Delta T}, & P_{\mathrm{ESS}} > 0 \\ \dfrac{\lambda_{\mathrm{sell}} \left(P_{\mathrm{ESS}} - \dfrac{P_{\mathrm{ESS}}}{\eta_{\mathrm{dis}}}\right)}{\Delta T}, & P_{\mathrm{ESS}} < 0 \end{cases} \tag{2.1}$$

where λ_{buy} is the real-time buying electricity price of the ESS; λ_{sell} is the real-time selling electricity price from the DC microgrid to the ESS; P_{ESS} is the measured power flow between the DC microgrid and the ESS; η_{ch} is the charging efficiency of the ESS, which is defined in [31] as

$$\eta_{\mathrm{ch}} = a_{\mathrm{ch}} - b_{\mathrm{ch}} P_{\mathrm{ESS}} \tag{2.2}$$

where a_{ch} and $b_{\mathrm{ch}}$are two linear coefficients to calculate the charging efficiency based on the power flow P_{ESS}; η_{dis} is the discharging efficiency of the ESS, which is also defined in [31] as

$$\eta_{\mathrm{dis}} = a_{\mathrm{dis}} + b_{\mathrm{dis}} P_{\mathrm{ESS}} \tag{2.3}$$

where a_{dis} and b_{dis} are two linear coefficients to calculate the discharging efficiency based on the power flow P_{ESS}.

By substituting (2.2) and (2.3) into (2.1), the operating cost of ESS can be derived as

$$C_{\mathrm{ESS}} = \begin{cases} \dfrac{\lambda_{\mathrm{buy}} \left[b_{\mathrm{ch}} P_{\mathrm{ESS}}^2 + (1 - a_{\mathrm{ch}}) P_{\mathrm{ESS}}\right]}{\Delta T}, & P_{\mathrm{ESS}} > 0 \\ \dfrac{\lambda_{\mathrm{sell}} \left[b_{\mathrm{dis}} P_{\mathrm{ESS}}^2 - (1 - a_{\mathrm{dis}}) P_{\mathrm{ESS}}\right]}{\Delta T \left(a_{\mathrm{dis}} + b_{\mathrm{dis}} P_{\mathrm{ESS}}\right)}, & P_{\mathrm{ESS}} < 0 \end{cases} \tag{2.4}$$

C. FUEL CELL COST

The operating cost of fuel cells can be calculated based on a quadratic relationship of the output power [32],

$$C_{\mathrm{FC}} = \frac{a_{\mathrm{FC}} P_{\mathrm{FC}}^2 + b_{\mathrm{FC}} P_{\mathrm{FC}} + c_{\mathrm{FC}}}{\Delta T} \tag{3}$$

where P_{FC} is the measured power flow between the DC microgrid and the fuel cell; a_{FC}, b_{FC}, and c_{FC} are constant coefficients.

D. DISTRIBUTION POWER LOSS COST

The power loss on the distribution lines is calculated based on the bus voltages, which are determined by the power flow of the entire DC microgrid rather than a specified power generation or consumption unit. However, due to the model of accurate power flow is a non-negligible constraint in the optimization problem, it can still be attributed to the utility cost in an explicit way. The operating cost of distribution power loss in this paper is defined as

$$C_{\mathrm{loss}} = \frac{\lambda_{\mathrm{buy}} P_{\mathrm{loss}}}{\Delta T} \tag{4}$$

where P_{loss} is the total power loss on the distribution lines.

III. OPERATING COST MODEL AND OPTIMIZATION

A. POWER FLOW MODEL

According to the applicability of droop control, DC microgrid buses can be categorized into non-dispatchable buses and dispatchable buses [25], [32], [33]. Non-dispatchable buses, also known as *P*-buses, are the buses with loads and non-dispatchable units, such as RES. Droop control is not applied for non-dispatchable units. Dispatchable buses are the buses with dispatchable units, such as utility grid, ESS, and fuel cells. Conventional droop control and its derivatives are widely adopted to equalize the output impedances of grid-connected converters of dispatchable units. Specifically, virtual resistances are designed in droop control for grid-connected converters to achieve active power balance. Fig. 2 shows the schematic diagram of conventional droop control for grid-connected converters of dispatchable units.

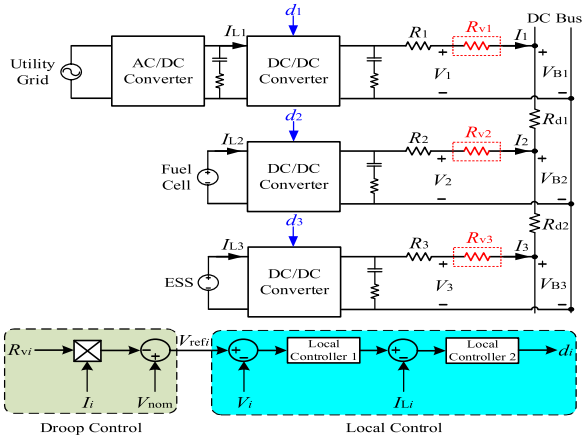

FIGURE 2. Schematic diagram of conventional droop control.

Here, R_i (i = 1, 2, 3) are the equivalent series resistances between the dispatchable units and the DC buses; R_{d1} and R_{d2} are the line resistances between the DC buses; $R_{\mathrm{v}i}$ (i = 1,2,3) are the virtual resistances of droop control to compensate the imbalance of the equivalent series resistances; V_i (i = 1,2,3) are the output voltages of the dispatchable units, which are controlled to track the nominal bus voltage V_{nom}; $V_{\mathrm{B}i}$ (i = 1,2,3) are the bus voltages; I_i (i = 1,2,3) are the output currents of the dispatchable units;

I_{Li} (i = 1,2,3) are the input currents of the DC/DC converters; d_i (i = 1,2,3) are the duty ratios of the DC/DC converters. Conventionally, R_{vi} are designed in the feedback control loop to compensate the imbalance of R_i, such that the output currents I_i are equally shared. However, in this paper, R_{vi} are optimized based on the operating cost model to reduce the total operating cost of DC microgrids. The optimized R_{vi} are further adopted for the feedback control in Fig. 2 to regulate the DC/DC converters. The local controller 1 generates the inductor current reference for the controller 2 based on the output voltage reference and the measured output voltage, whereas the controller 2 generates the duty ratios for the pulse-width-modulator to control the DC/DC converters based on the inductor current reference and the measured inductor current. In general, both the local controller 1 and the local controller 2 can be proportional-integral (PI) controllers.

Based on the Kirchhoff's law,

$$V_{Bi} = V_{nom} - R_{vi} I_i \tag{5.1}$$

where

$$I_i = \frac{P_{Di}}{V_{Bi}} \tag{5.2}$$

P_{Di} is the power provided/absorbed by the dispatchable unit i. By substituting (5.2) into (5.1), the power of dispatchable units can be expressed as

$$P_{Di} = -\frac{1}{R_{vi}} V_{Bi}^2 + \frac{V_{nom}}{R_{vi}} V_{Bi} \tag{5.3}$$

Besides, the DC microgrid is purely resistive at steady state, such that the injected current for all the non-dispatchable and dispatchable buses can be calculated based on the bus voltages and the admittances between the buses,

$$I_i = \sum_{j=1, j\neq i}^{n} Y_{ij} \left(V_{Bi} - V_{Bj}\right) \tag{6.1}$$

where Y_{ij} is the admittance between the bus i and the bus j.

The injected power for both non-dispatchable and dispatchable units are

$$P_i = V_{Bi} I_i \tag{6.2}$$

By substituting (6.1) into (6.2),

$$P_i = V_{Bi} \sum\nolimits_{j=1, j\neq i}^{n} Y_{ij} \left(V_{Bi} - V_{Bj}\right) \tag{6.3}$$

where n is the number of buses. Considering the active power balance of the DC microgrid,

$$P_i = P_{Di} + P_{Ni} + P_{Li} \tag{7}$$

where P_{Ni} are the power of non-dispatchable unit (i.e. RES power); P_{Li} are the power consumed by the load. Generally, profiles of P_{Ni} and P_{Li} are known.

Then, the power flow model of a DC microgrid can be formulated by (5.3) and (7), in which the number of total mismatch functions is

$$N = 2N_D + N_N \tag{8}$$

where N_D is the number of dispatchable buses; NN is the number of non-dispatchable buses. Due to the number of unknown variables (i.e. all the bus voltages and power of dispatchable units) equalizes the number of mismatch functions, the power flow of the DC microgrid has a unique solution, which can be solved by trust-region dogleg algorithms [4]. Besides, sensitivities of control parameters and power loss on the distribution lines can also be evaluated by the power flow model.

For a DC microgrid with the integrations of utility grids, RES, ESS, fuel cells, and loads, the active power is balanced at steady state

$$P_{RES} + P_U + P_{FC} + P_{ESS} = P_{load} + P_{loss} \tag{9}$$

where P_{RES} are the power supplied by the RES; and P_{load} are the power consumed by the loads.

B. OPERATING COST MODEL

The operating cost model allows the quantification and minimization of the total operating cost of the DC microgrid under real-time pricing, which can be expressed as

$$C_{total} = C_U + C_{ESS} + C_{FC} + C_{loss} \tag{10}$$

In this paper, the objective function is designed in positive correlation with the total operating cost (i.e., C_{total}), which means the smaller objective function value (i.e., J) resulting in lower totalt operating cost. To minimize the total operating cost, the objective function of the optimization is

$$\min J = C_{total}\left(R_{vi}, V_{Bi}, P_U, P_{ESS}, P_{FC}\right) \tag{11}$$

where the dependent variables V_{Bi}, P_U, P_{ESS}, and P_{FC} are calculated based on the power flow model and the independent variable R_{vi} in the optimization.

The constraints of the optimization include the constraints of power flow, bus voltages, and virtual resistances. The active power balance in (9) is one of the power flow constraints that restricts the overall power flow in the DC microgrid. Besides, the power of dispatchable units require to be strictly controlled within their respective capacity limits

$$P_{Umin} \leq P_U \leq P_{Umax} \tag{12}$$

$$P_{ESSmin} \leq P_{ESS} \leq P_{ESSmax} \tag{13}$$

$$0 \leq P_{FC} \leq P_{FCmax} \tag{14}$$

where P_{Umin} and P_{ESSmin} are the lower limits of P_U and P_{ESS}; P_{Umax}, P_{ESSmax} and P_{FCmax} are the upper limits of P_U, P_{ESS} and P_{FC}. Generally, P_{Umin} and P_{ESSmin} are negative, while P_{Umax}, P_{ESSmax} and P_{FCmax} are positive. The utility grid power (i.e. P_U) is mainly constrained by the current limits of the circuit breaker to implement over-current protection. The ESS power (i.e. P_{ESS}) is constrained to prolong the lifespan of ESS by prohibiting over-charge and -discharge. The fuel cell power (i.e. P_{FC}) is constrained to be positive and less than the upper limit to ensure safe operations. Moreover, according to the power grid standards in [33], the ESS is not allowed

to operate in the discharging mode when the DC microgrid injects power into the utility grid, such that

$$|P_{\mathrm{ESS}}| = \begin{cases} -P_{\mathrm{ESS}} & P_{\mathrm{U}} < 0 \\ |P_{\mathrm{ESS}}| & P_{\mathrm{U}} > 0 \end{cases} \tag{15}$$

Furthermore, bus voltages of the DC microgrid are required to be controlled within the limits,

$$V_{\mathrm{B}i\min} \le V_{\mathrm{B}i} \le V_{\mathrm{B}i\max} \tag{16}$$

According to the power flow model in (5.3) and (7), constraints of virtual resistances is

$$0 \le R_{\mathrm{v}i} \le R_{\mathrm{v}i\max} \tag{17}$$

where $R_{\mathrm{v}i\max}$ is the upper limit of $R_{\mathrm{v}i}$.

Therefore, the operating cost model of the DC microgrid is based on the objective function in (11), power flow constraints in (9), (12) $\sim$ (15), bus voltage constraints in (16), and virtual resistance constraints in (17).

C. HEURISTIC OPTIMIZATION BASED ON ADE

GA is a well-established heuristic algorithm to solve the optimization problems with multiple objectives and constraints [34]. However, the conventional GA is always running the risk of being trapped in a local optimum. The unstable performances of GA are frequently observed with strong randomness. Beyond that, it is hard to choose parameters such as the number of population size, generations, crossover rate, and mutation rate to guarantee the path to the optimal. Instead, ADE, as a stochastic direct search and global optimization algorithm developed by Storn and Price for continuous space optimization, can overcome the drawbacks of the conventional GA [35]. The advantages of ADE over the conventional GA can be concluded as follows [36]–[39]:

1) ADE can avoid being trapped in local optimum and outperforms conventional GA regarding single-objective and multiple-objective optimization problems;

2) ADE uses fewer tuning parameters than conventional GA. Only population size, maximum generation, differential weight (F) bounds and crossover rate (CR) bounds are adopted without resorting to an external probability density function;

3) ADE exhibits better performance in exploration and exploitation by dynamically adjusting F and CR.

In this paper, both the conventional GA and ADE are adopted to optimize the total operating cost of DC microgrids. For the conventional GA, the individuals (i.e. $R_{\mathrm{v}i}$) are randomly generated with the population size of P_{size}. Based on the fitness value of the objective function in (11) for each individual, two parent individuals are randomly selected to process crossover operator and mutation operator. If either of the terminal conditions of (i) the generations reaching the maximum generations or (ii) the algorithm being convergent, is satisfied, the GA stops and outputs the optimum solutions and the corresponding fitness value. On the contrary, if none of the terminal conditions is satisfied, the algorithm goes to the operations of selection, crossover, and mutation. The ADE algorithm consists of three stages, i.e., initialization stage, iteration stage, and the final stage.

Algorithm 1 Initialization

Input: dimension $dim(R_{\mathrm{v}})$, population size P_{size}, search space $(0, R_{\mathrm{vmax}})$

Output: initialized parent vector $\mathbf{R}$: yield of parent individual R_{vij}

```
Begin
    g ← 1    // g: generation number
    For i = 1: P_size    // i: individual number
        For j = 1 to dim    // j: individual dimension
            R_vi,j(g) = random (0, R_vmax)
            R ← R_vi,j(g)
        End
    End
    g ← g+1
End
```

1) INITIALIZATION STAGE

During this stage, the values of population size (P_{size}), generation maximum (max_{gen}) and stopping criteria in iterations are initialized. A random population of P_{size} individuals (R_{v}) is formed within the search-space bounds (i.e., $(0, R_{\mathrm{vmax}})$). We create an initialized solution with some attributes and methods in **Algorithm 1**.

2) ITERATION STAGE

For the conventional evolutionary algorithm (i.e., DE), the mutual operation performs at a low predefined probability (i.e., at 0.2) while the crossover operation is applied using a high value (i.e., 0.8). It is better to start with a high probability of mutation in the early generations and decrease it gradually. To achieve this, ADE adopts the adaptive mutual rate (p_{m}) and adaptive crossover rate (p_{c}), such that the algorithm is apt to more explorations of individual diversity in the early stage and is inclined to the exploitation afterwards.

The iteration stage of ADE comprises adaptive mutation, adaptive crossover, and selection operations. The main objective of mutation operation is to add some diversity by introducing more genetic materials into the population, to avoid the local optimum trap. For each individual $R_{\mathrm{v}i}$, mutation operation modifies $R_{\mathrm{v}i}$ by a small differential variation to create a mutant $R_{\mathrm{vm}i}$. As a result, the perturbation defines the direction and length of the search space. Specifically, three distinct individuals R_{vp1}, R_{vp2}, R_{vp3} are randomly selected with p1$\neq$ p2$\neq$ p3, and the difference vector, $R_{\mathrm{vp2}} - R_{\mathrm{vp3}}$, is calculated, the mutant individual $R_{\mathrm{vm}i}$ is then calculated as

$$R_{\mathrm{vm}i} = R_{\mathrm{vp1}} + p_{\mathrm{m}i}\left(R_{\mathrm{vp2}} - R_{\mathrm{vp3}}\right) \tag{18}$$

where $p_{\mathrm{m}i}\left(R_{\mathrm{vp2}} - R_{\mathrm{vp3}}\right)$ represents the mutation step size. All the mutants $R_{\mathrm{vm}i}$ are recorded in a mutant vector $\mathbf{Rm}$. $p_{\mathrm{m}i}$ is the mutation rate used to control the amplification of

the differential variation. Compared to the conventional DE of using a fixed value of p_m, the mutation rate of the ADE is adaptively generated for each individual as

$$p_{mi} = F_{min} + (F_{max} - F_{min})\frac{f_2 - f_1}{f_3 - f_1} \tag{19}$$

where F_{min} and F_{max} are the minimum and maximum mutation rate. f_1, f_2 and $f_3 (f_1 < f_2 < f_3)$ are the fitness values of $R_{vp1}(g), R_{vp2}(g), R_{vp3}(g)$ based on the objective function (11).

Then, the crossover operator amalgamates the mutant vector **Rm** and the parent vector **R** to create a trial vector **Rt**. Generally, the crossover operation can be implemented in either binomial or exponential. Due to that the binomial is more straightforward and more frequently used, it is adopted for the crossover operation in this paper as

$$R_{vti} = \begin{cases} R_{vmi}, & r < p_{ci} \\ R_{vi}, & \text{others} \end{cases} \tag{20}$$

where $r \sim N(0,1)$ is a normal distribution. All the trail individuals R_{vti} are recorded in a trial vector **Rt**. Each offspring is a stochastic linear combination of three randomly selected individuals when $r < p_{ci}$. Otherwise, the offspring inherits from the parent vector. Superior to the conventional DE of using a fixed value of p_c, the crossover rate of the ADE is adaptively generated for each individual as

$$p_{ci} = \begin{cases} p_{min} + \dfrac{(p_{max} - p_{min})(f_i - f_{min})}{f_{max} - f_{min}}, & f_i < f \\ p_{min}, & f_i \geq f \end{cases} \tag{21}$$

where p_{min} and p_{max} are the minimum and maximum crossover rate. f_{min}, f_{max} and f are the minimum, maximum and average objectives of $R_{vp1}(g), R_{vp2}(g), R_{vp3}(g)$. f_i is the fitness values of the current individual. Since the crossover rate p_{ci} is adaptive, it makes better offsprings more likely to be survived next generation compared to the fixed crossover rate. The successful crossover rate of the last generation would be used to guide the generation of new offspring. Pseudocodes of the adaptive mutation and crossover operations of ADE are shown in **Algorithms 2** and **3**.

The third operation of ADE in the iteration stage is selection, which is similar to the elitism operation of the conventional GA. Selection operation is conducted based on one-to-one competition between the individuals in the parent vector and the trial vector at every generation. Better individuals are chosen for the next generation. Specifically, if the fitness value of the objective function based on the trial vector is less than or equal to that of the parent vector **R**, the trial vector will survive and be used for the next generation. Otherwise, the parent vector will be adopted for the next generation. Pseudocode of the selection of ADE is described in **Algorithm 4**.

3) FINAL STAGE

Two terminal criteria of ADE include the maximum generation max_{gen} and the maximum deviation rate max_{dr}. In the final stage, the algorithm stops when any one of the terminal criteria is satisfied.

By considering all the stages of ADE, pseudocode of the entire algorithm is presented in **Algorithm 5**.

Algorithm 2 Mutation Operation

Input: mutation rate bound (F_{min}, F_{max}), population size P_{size}, parent vector **R**
Output: mutant vector **Rm**: yield of offspring R_{vmi}

```
Begin
  g ← 1
  For i = 1: P_size
    While (p1 = p2 or p1 = p3 or p2 = p3) do
      Select R_vp1(g), R_vp2(g), R_vp3(g) from R(g)
    End
    Rvmi(g) = Rvp1 (g) + pmi(Rvp2 (g) − Rvp3 (g))
    Rm ← R_vm(g)
  End
  g ← g+1
End
```

Algorithm 3 Crossover Operation

Input: crossover rate bound (P_{min}, P_{max}), mutant vector **Rm**, population size P_{size}
Output: trial vector **Rt**: yield of offspring R_{vti}

```
Begin
  g ← 1
  For i = 1: P_size
    If r < p_ci, then R_vti(g) = R_vmi(g) else R_vti(g) = R_vi(g)
    Rt ← R_vti(g)
  End
  g ← g+1
End
```

IV. CASE STUDIES

Two cases are studied in this paper to validate the generality of ADE algorithm to reduce the operating cost of DC microgrids. Cases 1 is carried out on a 12-bus 380V meshed DC microgrid using Matlab, while case 2 is conducted on a 32-bus 380V DC meshed DC microgrid using a Real-Time Digital Simulator (RTDS).

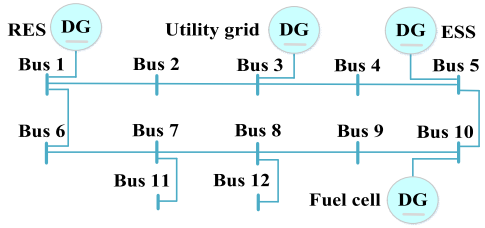

FIGURE 3. Structure of the 12-bus 380V meshed DC microgrid.

A. CASE 1: 12-BUS DC MICROGRID

The structure of the 12-bus DC microgrid is plotted in Fig. 3. Buses 3, 5, and 10 are three dispatchable buses that are

Algorithm 4 Selection Operation

Input: trial vector **Rt**, parent vector **R**, population size P_{size}
Output: optimum vector **R**: yield of optimum individual R_{vi}

1. Begin
2. $g \leftarrow 1$
3. For $i = 1$: P_{size}
4. If $f\ (R_{\text{vt}i}(\text{g})) <= R_{vi}(\text{g})$, then $R_{v(i+1)}(g) = R_{\text{vt}i}(g)$ else $R_{v(i+1)}(g) = R_{vi}(g)$
5. $\mathbf{R} \leftarrow R_{\text{vt}i}(g)$
6. End
7. $g \leftarrow g+1$
8. End

Algorithm 5 The ADE Algorithm

Input: dimension $dim(R_{\text{vi}})$, population size P_{size}, crossover rate bound ($P_{\min}$, $P_{\max}$), mutation rate bound ($F_{\min}$, $F_{\max}$), maximum generation max_{gen}, maximum deviation rate max_{dr}
Output: optimal solutions R_{vi}, optimal fitness J

1. **Begin**
2. $g \leftarrow 1$ // g: generation number
3. \\ **Initialization**
4. $R_{\text{vi}}(\text{g}) = \text{initialization}\ ();$
5. \\ **Iteration**
6. **While** the terminal criteria not met **do**
7. $J = \text{fitness}\ (R_{\text{v}i}(g));$ // J: fitness of the objective function
8. // **mutation operation** $R_{\text{vm}i}(g) = \text{mutation}\ (R_{\text{v}i}(g))$
9. $J = \text{fitness}\ (R_{\text{mv}i}(g))$
10. // **crossover operation** $R_{\text{vt}i}(g) = \text{crossover}\ (R_{\text{v}i}(\text{g}), R_{\text{vm}i}(\text{g}))$
11. $J = \text{fitness}\ (R_{\text{vt}i}(g))$
12. // **selection operation** $R_{\text{v}i}(\text{g}) = \text{selection}\ (R_{\text{v}i}(g), R_{\text{vt}i}(g))$
13. **End while**
14. \\ **The final stage**
15. Output optimal solution $R_{\text{v}i}$; optimal fitness J
16. **End**

TABLE 1. Line impedances of the 12-bus dc microgrid.

From Bus	To Bus	R_{line} (Ω)	From Bus	To Bus	R_{line} (Ω)
1	2	0.566	8	9	0.491
2	3	0.559	9	10	0.498
3	4	0.571	1	6	0.660
4	5	0.558	7	11	0.661
6	7	0.496	8	12	0.658
7	8	0.495	5	10	0.665

TABLE 2. Parameters for operating cost calculation.

Parameter	Value	Parameter	Value	Parameter	Value
a_{ch}	0.92	b_{ch}	0.01	a_{dis}	0.85
b_{dis}	0.015	a_{FC}	0.00715	b_{FC}	2.07
c_{FC}	20	ΔT	1000		

TABLE 3. Constraints of the parameters.

Parameter	Lower Limit	Upper Limit
P_{U}	P_{Umin}=−30 kW	P_{Umax}=30 kW
P_{ESS}	P_{ESSmin}=−30 kW	P_{ESSmax}=30 kW
P_{FC}	P_{FCmin}=0 kW	P_{FCmax}=30 kW
$V_{\text{B}i}$	$V_{\text{B}i\text{min}}$=342 V	$V_{\text{B}i\text{max}}$=418 V
$R_{\text{V}i}$	$R_{\text{V}i\text{min}}$=0 Ω	$R_{\text{V}i\text{max}}$=1 Ω

TABLE 4. Parameters of the GA.

Parameter	Value	Parameter	Value
P_{size}	12	max_{gen}	1000
Mutation rate	0.2	Crossover rate	0.9
Selection rate	0.5		

TABLE 5. Parameters of the ADE.

Parameter	Value	Parameter	Value
P_{size}	18	max_{gen}	400
$F_{\min}$	0.1	$F_{\max}$	0.8
$P_{\min}$	0.1	$P_{\max}$	0.6

interfaced with a utility grid, ESS, and fuel cells. Bus 1 is a non-dispatchable bus that is interfaced with RES. The rest buses are non-dispatchable buses contributing to feeding loads. Line resistances of the DC microgrid, parameters of the components to calculate their operating cost, and constraints of power flow, bus voltages, and virtual resistances, are listed in Tables 1∼3, respectively. The parameters of the conventional GA and ADE, which are selected by taking both optimization accuracy and computation time into consideration, are provided in Tables 4 and 5, respectively. The 24-hour power profiles of the RES at the bus 1 and the loads at the buses 2, 4, 6, 7, 8, 9, 11, and 12 are plotted in Fig. 4. Real-time electricity prices (λ_{buy} and λ_{sell} are assumed to be equal) are obtained from Open Energy Information [40], which are plotted in Fig. 5.

Initially, to verify the convergence of ADE, the total operating cost of the 12-bus DC microgrid at every hour are optimized based on the power profiles in Fig. 4 and the electricity prices in Fig. 5. The initial virtual resistances for all the dispatchable units are 0.5 Ω. The total operating cost is converged within short periods, which are less than 2 seconds Fig. 6. shows the convergence traces of ADE from 1-hour to 8-hour (Due to the page limit, convergence trances from 9-hour to 24-hour are not shown in the paper. TOC is the acronym of total operating cost). Compare to one hour, the computation time of ADE is negligible. Then, the total

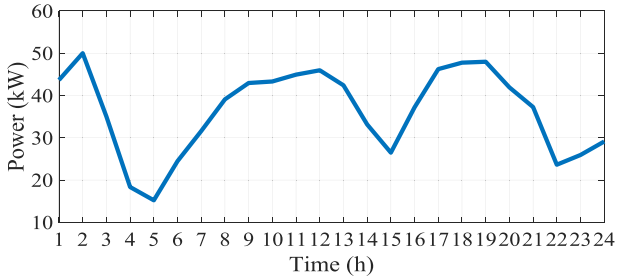

(a) 24-hour power profiles of RES

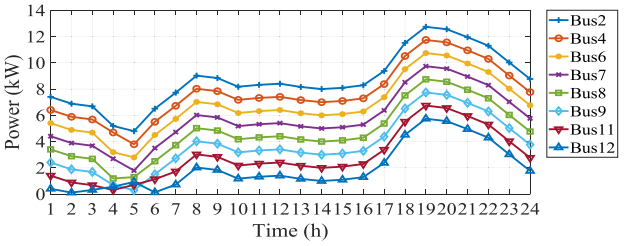

(b) loads of the 12-bus

FIGURE 4. 24-hour power profiles of RES and loads of the 12-bus microgrid.

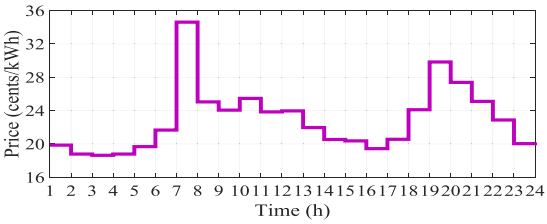

FIGURE 5. Real-time pricing profile.

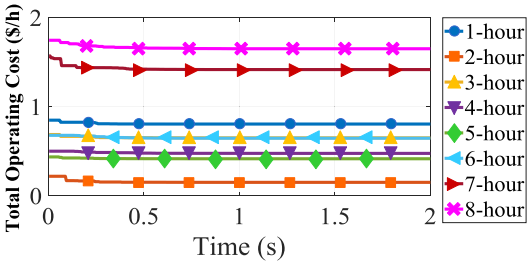

FIGURE 6. Convergence traces of ADE from 1-hour to 8-hour.

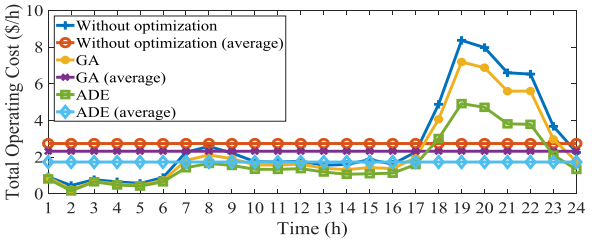

FIGURE 7. Total operating cost of the 12-bus DC microgrid without optimization, with the optimization of GA and ADE.

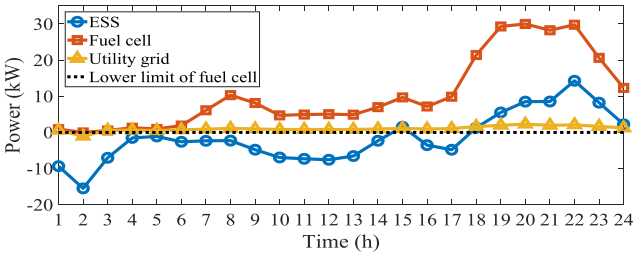

FIGURE 8. Power of dispatchable units in the 12-bus DC microgrid with ADE.

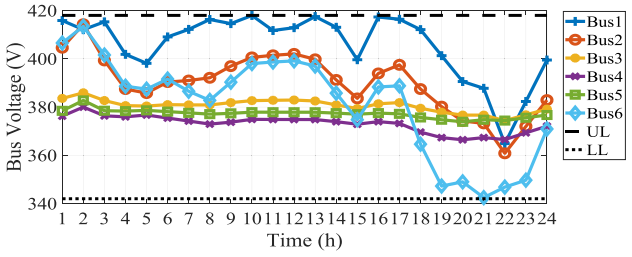

(a) bus 1~6

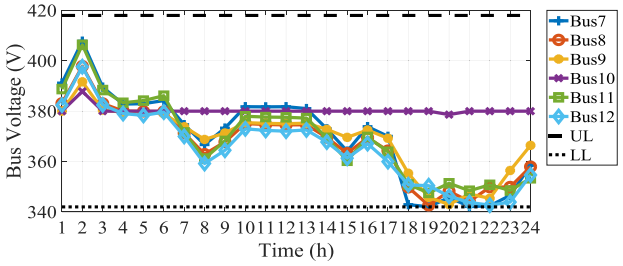

(b) bus 7-12

FIGURE 9. Bus voltages of the 12-bus DC microgrid with ADE.

operating cost of the 12-bus DC microgrid without optimization and with the optimization of GA are also conducted. The comparisons of the total operating cost among the microgrid without optimization, with the optimization of GA, and ADE are presented in Fig. 7.

Compared to the microgrid without optimization, the microgrid with the optimization of GA can reduce the total operating cost at every hour. The average operating cost per hour are 2.74 \$/h and 2.32 \$/h (1 \$ = 100 cents) for the microgrid without optimization and with the optimization of GA, respectively. The cost reduction by using GA is about 15.33%. The total operating cost can be further reduced by the optimization of ADE at every hour. The average operating cost per hour of the microgrid can be reduced to 1.73 \$/h with the optimization of ADE, which is about 36.86% and 25.43% reduction as compared to the microgrid without optimization and with the optimization of GA. Accordingly, the power of dispatchable units and the bus voltages of the microgrid with the optimization of ADE are presented in Figs. 8 and 9, respectively.

Here, UL and LL indicate the upper and lower limits of the bus voltages. Obviously, the power and bus voltages

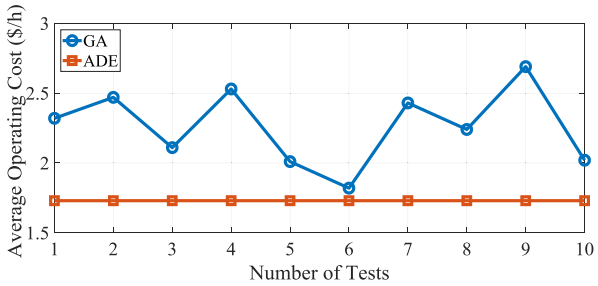

FIGURE 10. Ten-times average operating cost per hour for both algorithms.

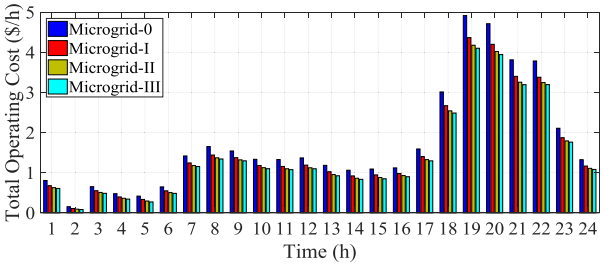

FIGURE 11. Total operating cost of various 12-bus DC microgrids with ADE.

at every hour are within the tolerances. Besides, compared to the high randomness of the conventional GA, ADE is a much steadier algorithm, which ensures the consistency of the minimum operating cost of the microgrid. To verify this, the optimization with GA and ADE are conducted ten times independently. Fig. 10 shows the ten-times average operating cost per hour for both algorithms. ADE is more stable in virtue of the standard deviation is zero, while GA varies with a standard deviation of 0.273.

Moreover, based on the structure of the microgrid in Fig. 3 (i.e. microgrid-0), an ESS is integrated at bus 6. As a result, bus 6 is changed from non-dispatchable to dispatchable. The total operating cost of the altered DC microgrid (i.e. microgrid-I) is optimized by GA and ADE. The average total operating cost per hour of the microgrid with the optimization of ADE can be reduced about 40.33% and 28.12%, as compared to the microgrid without optimization and with the optimization of GA. The power of dispatchable units and the bus voltages for the microgrid with the optimization of ADE are within the tolerances. Compare the total operating cost of the microgrid-I with the optimization of ADE to the counterparts of the microgrid-0 in Fig. 7, the total operating cost at every hour are further reduced, as shown in Fig. 11. The average operating cost per hour is reduced about 11.99% (from 1.73 \$/h to 1.522 \$/h). Furthermore, a utility grid is interfaced at bus 11 of the microgrid-I to become microgrid-II. The total operating cost at every hour of the microgrid-II with the optimization of ADE is lower than the counterparts of the microgrid-I, as shown in Fig. 11. The average operating cost per hour is reduced about 5.01% (from 1.522 \$/h to 1.446 \$/h). Then, fuel cells are integrated at bus 12 of the microgrid-II to become microgrid-III. The total operating cost at every hour of the microgrid-III with the optimization of ADE are lower than the counterparts of the microgrid-II, as shown in Fig. 11. The average total operating cost is reduced about 2.27% (from 1.446 \$/h to 1.413 \$/h). The cost saving for DC microgrids with the optimization of ADE is more prominent when the dispatchable units are expanded.

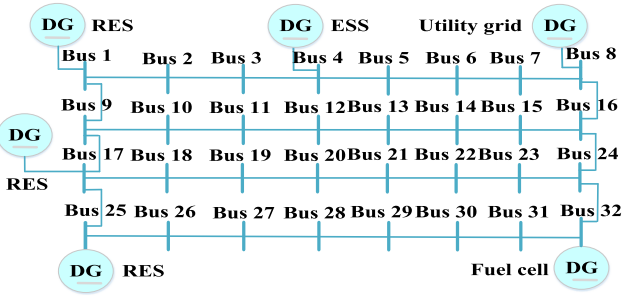

FIGURE 12. Structure of the 32-bus 380V meshed DC microgrid.

B. CASE 2: 32-BUS DC MICROGRID

Case studies are also carried out on a 32-bus 380V meshed DC microgrid built in RSCAD and tested using a Real-Time Digital Simulator (RTDS) to validate that the proposed method is universally applicable to DC microgrids and more operating cost can be reduced when more dispatchable units are connected. The structure of the 32-bus DC microgrid is plotted in Fig. 12. Buses 4, 8, and 32 are three dispatchable buses. Buses 1, 17, and 25 are three non-dispatchable buses with RES. The rest buses are non-dispatchable buses contributing to feeding loads. Line resistances of the 32-bus DC microgrid are listed in Table 6. The parameters for operating cost calculation, the constraints, and the parameters of the conventional GA and ADE are identical to those of the 12-bus microgrid in Tables 2∼5. The 24-hour power profiles of RES and loads are plotted in Fig. 13. Real-time electricity prices are the same as the electricity prices in Fig. 5.

The optimization of the 32-bus DC microgrid by the conventional GA and the ADE are conducted offline. The obtained optimal virtual resistances are modelled in the 32-bus microgrid in RSCAD. The total operating cost at every hour of the 32-bus microgrid without optimization, with the optimization of GA, and ADE are presented in Fig. 14. Compared to the microgrid without optimization and with the optimization of GA, the total operating cost of the microgrid with the optimization of ADE can be reduced at every hour. The average operating cost per hour are reduced about 23.75% (from 3.422 \$/h to 2.609 \$/h) and 10.97% (from 2.931 \$/h to 2.609 \$/h) by the ADE, respectively. Besides, with more integrations of dispatchable units, more operating cost reduction can be achieved by the ADE, as shown in Fig. 15. The average operating cost per hour is reduced about 12.49% (from 2.609 \$/h to 2.284 \$/h) when an ESS is interfaced at the bus 24 (microgrid-I). The average operating

TABLE 6. Line impedances of the 32-bus dc microgrid.

From Bus	To Bus	R_{line} (Ω)	From Bus	To Bus	R_{line} (Ω)
1	2	0.561	20	21	0.495
2	3	0.561	21	22	0.495
3	4	0.561	22	23	0.495
4	5	0.561	23	24	0.495
5	6	0.561	25	26	0.561
6	7	0.561	26	27	0.561
7	8	0.561	27	28	0.561
9	10	0.495	28	29	0.561
10	11	0.495	29	30	0.561
11	12	0.495	30	31	0.561
12	13	0.495	31	32	0.561
13	14	0.495	1	9	0.660
14	15	0.495	8	16	0.660
15	16	0.495	9	17	0.660
17	18	0.495	16	24	0.660
18	19	0.495	17	25	0.660
19	20	0.495	24	32	0.660

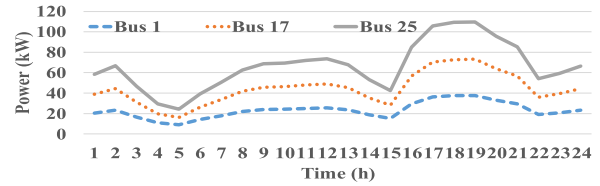

(a) RES power profile

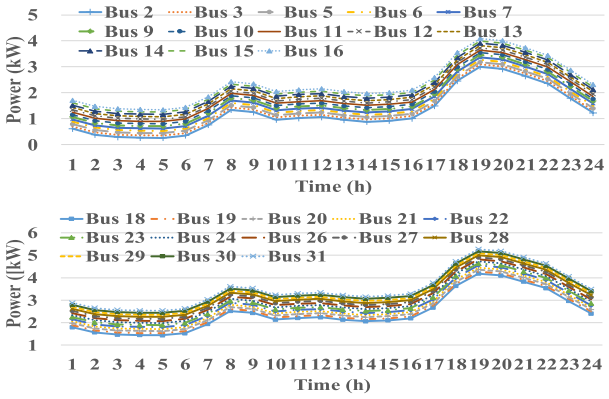

(b) load power profile

FIGURE 13. 24-hour power profiles of RES and loads for the 32-bus DC microgrid.

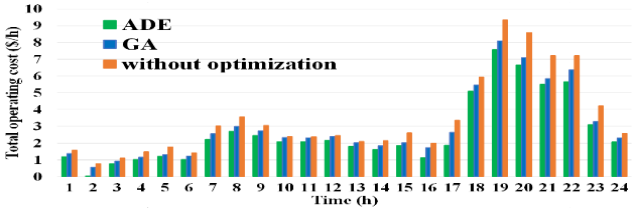

FIGURE 14. Total operating cost of the 32-bus DC microgrid without optimization, with the optimization of GA and ADE.

cost per hour are further reduced about 6.2% (from 2.284 $/h to 2.142 $/h), 3.54% (from 2.142 $/h to 2.066 $/h), and 1.34% (from 2.066 $/h to 2.038 $/h) when the integrations

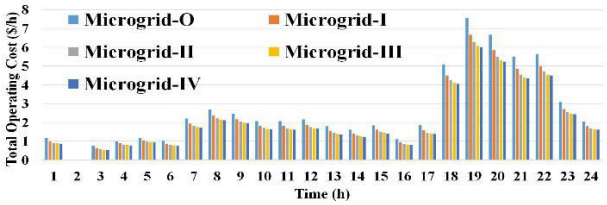

FIGURE 15. Total operating cost of various 32-bus DC microgrids with ADE.

of a utility grid at the bus 28 (microgrid-II), fuel cells at bus 13 (microgrid-III), an ESS at bus 19 (microgrid-IV).

V. CONCLUSION

This paper presents an ADE-based optimization scheme for DC microgrids to reduce the total operating cost under real-time pricing. The ADE optimizes the virtual resistances of dispatchable units, such that the power flow of DC microgrids can be regulated to minimize the total operating cost. Case studies of a 12-bus DC microgrid in simulation validate the microgrid with the optimization of ADE can be reduced about 40.33% and 28.12% average operating cost per hour, as compared to the microgrid without optimization and with the optimization of GA. Besides, with more integrations of dispatchable units, the total operating cost reduction by ADE are more significant. The average operating cost per hour is sequentially reduced about 11.99%, 5.01%, and 2.27% for the 12-bus DC microgrid from with 3 dispatchable units to with 4, 5, and 6 dispatchable units. Case studies of a 32-bus DC microgrid using an RTDS also demonstrate the ADE can reduce the average operating cost per hour about 23.75% and 10.97%, as compared to the microgrid without optimization and with GA, respectively. The average operating cost per hour of 32-bus DC microgrids with ADE is sequentially reduced about 12.49%, 6.2%, 3.54%, and 1.34% from with 6 dispatchable units to with 7, 8, 9, and 10 dispatchable units.

REFERENCES

[1] J. M. Guerrero, J. C. Vasquez, J. Matas, L. García de Vicuna, and M. Castilla, "Hierarchical control of droop-controlled AC and DC microgrids—A general approach toward standardization," *IEEE Trans. Ind. Electron.*, vol. 58, no. 1, pp. 158–172, Jan. 2011.

[2] Y. Ito, Y. Zhongqing, and H. Akagi, "DC microgrid based distribution power generation system," in *Proc. 4th Int. Power Electron. Motion Control Conf. (IPEMC)*, Xi'an, China, Aug. 2004, pp. 1740–1745.

[3] Y. Yang, K.-T. Mok, S.-C. Tan, and S. Y. Hui, "Nonlinear dynamic power tracking of low-power wind energy conversion system," *IEEE Trans. Power Electron.*, vol. 30, no. 9, pp. 5223–5236, Sep. 2015.

[4] C. Li, S. K. Chaudhary, M. Savaghebi, J. C. Vasquez, and J. M. Guerrero, "Power flow analysis for low-voltage AC and DC microgrids considering droop control and virtual impedance," *IEEE Trans. Smart Grid*, vol. 8, no. 6, pp. 2754–2764, Nov. 2017.

[5] H. Farhangi, "The path of the smart grid," *IEEE Power Energy Mag.*, vol. 8, no. 1, pp. 18–28, Jan. 2010.

[6] J. Deng, Y. Mao, and Y. Yang, "Distribution power loss reduction of standalone DC microgrids using adaptive differential evolution-based control for distributed battery systems," *Energies*, vol. 13, no. 9, p. 2129, Apr. 2020.

[7] P. Karlsson and J. Svensson, "DC bus voltage control for a distributed power system," *IEEE Trans. Power Electron.*, vol. 18, no. 6, pp. 1405–1412, Nov. 2003.
[8] K. Strunz, E. Abbasi, and D. N. Huu, "DC microgrid for wind and solar power integration," *IEEE J. Emerg. Sel. Topics Power Electron.*, vol. 2, no. 1, pp. 115–126, Mar. 2014.
[9] Y. Yang, Y. Qin, S.-C. Tan, and S. Y. R. Hui, "Efficient improvement of photovoltaic-battery systems in standalone DC microgrids using a local hierarchical control for the battery system," *IEEE Trans. Power Electron.*, vol. 34, no. 11, pp. 10796–10807, Nov. 2019.
[10] L. Meng, T. Dragicevic, J. Roldán-Pérez, J. C. Vasquez, and J. M. Guerrero, "Modeling and sensitivity study of consensus algorithm-based distributed hierarchical control for DC microgrids," *IEEE Trans. Smart Grid*, vol. 7, no. 3, pp. 1504–1515, May 2016.
[11] P. Wang, X. Lu, X. Yang, W. Wang, and D. Xu, "An improved distributed secondary control method for DC microgrids with enhanced dynamic current sharing performance," *IEEE Trans. Power Electron.*, vol. 31, no. 9, pp. 6658–6673, Sep. 2016.
[12] Y. Jiang, Y. Yang, S.-C. Tan, and S.-Y.-R. Hui, "Adaptive current sharing of distributed battery systems in DC microgrids using adaptive virtual resistance-based droop control," in *Proc. IEEE Energy Convers. Congr. Expo. (ECCE)*, Baltimore, MD, USA, Sep. 2019, pp. 4262–4267.
[13] X. Lu, K. Sun, J. M. Guerrero, J. C. Vasquez, and L. Huang, "State-of-charge balance using adaptive droop control for distributed energy storage systems in DC microgrid applications," *IEEE Trans. Ind. Electron.*, vol. 61, no. 6, pp. 2804–2815, Jun. 2014.
[14] Y. Yang, S.-C. Tan, and S. Y. R. Hui, "Mitigating distribution power loss of DC microgrids with DC electric springs," *IEEE Trans. Smart Grid*, vol. 9, no. 6, pp. 5897–5906, Nov. 2018.
[15] I. U. Nutkani, W. Peng, P. C. Loh, and F. Blaabjerg, "Cost-based droop scheme for DC microgrid," in *Proc. IEEE Energy Convers. Congr. Expo. (ECCE)*, Pittsburgh, PA, USA, Sep. 2014, pp. 765–769.
[16] M. Zaery, E. M. Ahmed, and M. Orabi, "Low operational cost distributed prioritised coordinated control for DC microgrids," *IET Smart Grid*, vol. 2, no. 2, pp. 233–241, Jun. 2019.
[17] Z. Wang, W. Wu, and B. Zhang, "A distributed control method with minimum generation cost for DC microgrids," *IEEE Trans. Energy Convers.*, vol. 31, no. 4, pp. 1462–1470, Dec. 2016.
[18] J. Hu, J. Duan, H. Ma, and M.-Y. Chow, "Distributed adaptive droop control for optimal power dispatch in DC microgrid," *IEEE Trans. Ind. Electron.*, vol. 65, no. 1, pp. 778–789, Jan. 2018.
[19] H. Han, H. Wang, Y. Sun, J. Yang, and Z. Liu, "Distributed control scheme on cost optimisation under communication delays for DC microgrids," *IET Gener., Transmiss. Distrib.*, vol. 11, no. 17, pp. 4193–4201, Nov. 2017.
[20] S. Moayedi and A. Davoudi, "Unifying distributed dynamic optimization and control of islanded DC microgrids," *IEEE Trans. Power Electron.*, vol. 32, no. 3, pp. 2329–2346, Mar. 2017.
[21] S. Kır, H. R. Yazgan, and E. Tüncel, "A novel heuristic algorithm for capacitated vehicle routing problem," *J. Ind. Eng. Int.*, vol. 13, no. 3, pp. 323–330, Feb. 2017.
[22] I. Podlubny, *Fractional Differential Equations—An Introduction to Fractional Derivatives, Fractional Differential Equations, to Methods of Their Solution and Some of Their Applications*, vol. 198. Amsterdam, The Netherlands: Elsevier, Oct. 1998, pp. 1–340.
[23] S. Sreenivas and K. Vijaya, "A review on non-traditional optimization algorithm for simultaneous scheduling problems," *J. Mech. Civil Eng.*, vol. 12, no. 2, pp. 50–53, Mar. 2015.
[24] S. A. Cook, "An overview of computational complexity," *Commun. ACM*, vol. 26, no. 6, pp. 400–408, Jun. 1983.
[25] C. Li, F. de Bosio, F. Chen, S. K. Chaudhary, J. C. Vasquez, and J. M. Guerrero, "Economic dispatch for operating cost minimization under real-time pricing in droop-controlled DC microgrid," *IEEE J. Emerg. Sel. Topics Power Electron.*, vol. 5, no. 1, pp. 587–595, Mar. 2017.
[26] C. Chen, S. Duan, T. Cai, B. Liu, and G. Hu, "Optimal allocation and economic analysis of energy storage system in microgrids," *IEEE Trans. Power Electron.*, vol. 26, no. 10, pp. 2762–2773, Oct. 2011.
[27] A. A. Hamad and E. F. El-Saadany, "Multi-agent supervisory control for optimal economic dispatch in DC microgrids," *Sustain. Cities Soc.*, vol. 27, pp. 129–136, Nov. 2016.
[28] E. Planas, J. Andreu, J. I. Gárate, I. Martínez de Alegría, and E. Ibarra, "AC and DC technology in microgrids: A review," *Renew. Sustain. Energy Rev.*, vol. 43, pp. 726–749, Mar. 2015.
[29] *The Intelligent Energy System of the Future*, Danish Ministry of Climate, Energy and Building, Smart Grid Strategy, Copenhagen, Denmark, 2013.
[30] *A Report on Promoting Wind and Photovoltaic Power With Flat Trades Online From The NDRC (National Development and Reform Commission)*. Accessed: Jul. 2020. [Online]. Available: https://www.ndrc.gov.cn/xxgk/zcfb/tz/202008/t20200805_1235592.html
[31] Y. Xu, W. Zhang, G. Hug, S. Kar, and Z. Li, "Cooperative control of distributed energy storage systems in a microgrid," *IEEE Trans. Smart Grid*, vol. 6, no. 1, pp. 238–248, Jan. 2015.
[32] M. Y. Nguyen and Y. T. Yoon, "A comparison of microgrid topologies considering both market operations and reliability," *Electr. Power Compon. Syst.*, vol. 42, no. 6, pp. 585–594, Mar. 2014.
[33] T. Ersal, C. Ahn, D. L. Peters, J. W. Whitefoot, A. R. Mechtenberg, I. A. Hiskens, H. Peng, A. G. Stefanopoulou, P. Y. Papalambros, and J. L. Stein, "Coupling between component sizing and regulation capability in microgrids," *IEEE Trans. Smart Grid*, vol. 4, no. 3, pp. 1576–1585, Sep. 2013.
[34] D. Whitley, "A genetic algorithm tutorial," *Statist. Comput.*, vol. 4, no. 2, pp. 65–85, Jun. 1994.
[35] R. Storn and K. Price, "Differential evolution-a simple and efficient heuristic for global optimization over continuous spaces," *J. Global Optim.*, vol. 11, no. 4. Dordrecht, The Netherlands: Springer, 1997, pp. 341–359.
[36] T. Tušar and B. Filipič, "Differential evolution versus genetic algorithms in multiobjective optimization," in *Evolutionary Multi-Criterion Optimization*, Mar. 2007, pp. 257–271.
[37] Y. Yang, S.-C. Tan, and S. Y. R. Hui, "Front-end parameter monitoring method based on two-layer adaptive differential evolution for SS-compensated wireless power transfer systems," *IEEE Trans. Ind. Informat.*, vol. 15, no. 11, pp. 6101–6113, Nov. 2019.
[38] Y. Mao, S. Niu, and Y. Yang, "Differential evolution-based multiobjective optimization of the electrical continuously variable transmission system," *IEEE Trans. Ind. Electron.*, vol. 65, no. 3, pp. 2080–2089, Mar. 2018.
[39] J. Brest, V. Zumer, and M. S. Maucec, "Self-adaptive differential evolution algorithm in constrained real-parameter optimization," in *Proc. IEEE Int. Conf. Evol.*, Vancouver, BC, Canada, Jul. 2006, pp. 215–222.
[40] *Open Energy Information (OpenEI)*. [Online]. Available: http://en.openei.org

XIAOYAN QIAN (Student Member, IEEE) received the B.Eng. degree in industrial engineering from the Zhejiang University of Technology, Zhejiang, China, in 2013, and the M.Eng. degree in industrial engineering from Zhejiang Sci-Tech University, Zhejiang, in 2016. She is currently pursuing the Ph.D. degree with the Department of Electrical and Electronic Engineering, The University of Hong Kong. Her current research interests include intelligent evolutionary algorithms, deep neural networks, and applications of these methods to DC microgrid systems.

YUN YANG (Member, IEEE) received the B.S. degree in electrical engineering from Wuhan University, Wuhan, China, in 2012, and the Ph.D. degree in power electronics from the Department of Electrical and Electronic Engineering, The University of Hong Kong, Hong Kong, in 2017. From November 2017 to August 2020, he was a Postdoctoral Research Fellow with the Department of Electrical and Electronic Engineering, The University of Hong Kong. He is currently a Research Assistant Professor with the Department of Electrical Engineering, The Hong Kong Polytechnic University, Hong Kong. His research interests include wireless power transfer, microgrids, and power electronics and control.

CHENDAN LI (Member, IEEE) received the B.S. degree in electrical engineering from Nanjing Agricultural University, Nanjing, China, in 2009, the M.S. degree in electrical engineering from the Nanjing University of Aeronautics and Astronautics, Nanjing, in 2012, and the Ph.D. degree from Aalborg University, Denmark, in 2016. She is currently a Postdoctoral Fellow with the Department of Electric Power Engineering, Norwegian University of Science and Technology (NTNU). Her main research interests include analysis and control for AC and DC microgrids, operation of distribution systems, and control and operation of power electronics-based power systems. She serves as an Associate Editor on the editorial board for *Electrical Engineering* (Springer).

SIEW-CHONG TAN (Senior Member, IEEE) received the B.Eng. (Hons.) and M.Eng. degrees in electrical and computer engineering from the National University of Singapore, Singapore, in 2000 and 2002, respectively, and the Ph.D. degree in electronic and information engineering from The Hong Kong Polytechnic University, Hong Kong, in 2005. He was a Visiting Scholar with the Grainger Center for Electric Machinery and Electromechanics, University of Illinois at Urbana-Champaign, Champaign, from September to October 2009. He was also an Invited Academic Visitor with the Huazhong University of Science and Technology, Wuhan, China, in December 2011. He is currently a Professor with the Department of Electrical and Electronic Engineering, The University of Hong Kong, Hong Kong. He is the coauthor of the book *Sliding Mode Control of Switching Power Converters: Techniques and Implementation* (Boca Raton: CRC, 2011). His research interests include power electronics and control, smart grids, and clean energy technologies. He serves as an Associate Editor for the IEEE TRANSACTIONS ON POWER ELECTRONICS.